SUPPORT OF ICING FLIGHT TESTS BY NEAR REAL-TIME DATA ANALYSIS

C. Raab, P. Ohme, C. Deiler
DLR, Institute of Flight Systems
Lilienthalplatz 7, 38108 Braunschweig, Germany

Abstract

Flight testing of aircraft with altered aerodynamic configuration is a safety critical and time consuming task. For the evaluation of the aircraft characteristics under SLD icing conditions, flight tests with artificial ice shapes were performed. These flight tests were supported by online algorithms for the estimation of aerodynamic parameters. Results were available in near real-time onboard the aircraft or already during the debriefing on ground. Pre-flight data from wind tunnel experiments could be confirmed already during the flight using these online analysis tools, thus the flight tests could be performed in shorter time and more safe. This paper will introduce the developed analysis tools and will present results from the flight test campaign.

NOMENCLATURE

a_x, a_y, a_z	Translational accelerations along the body axes	m/s²
C_X, C_Y, C_Z	Aerodynamic force coefficients in body axes	-
C_l, C_m, C_n	Aerodynamic moment coefficients in body axes	-
C_L	Aerodynamic lift coefficient	-
C_D	Aerodynamic drag coefficient	-
I_{xx}, I_{yy}, I_{zz}	Roll, pitch and yaw moments of inertia	kgm²
I_{xz}	Product of inertia	kgm²
l_μ	Mean aerodynamic chord	m
M_x, M_y, M_z	Engine thrust moments in body axes	Nm
m	Total aircraft mass	kg
p, q, r	Roll, pitch and yaw rate	rad/s
$\bar{q}$	Dynamic pressure	N/m²
s	Half of the wing span	m
S	Reference wing area	m²
sp_{avg}	Average spoiler deflection	rad
sp_{diff}	Differential spoiler deflection	rad
T_x, T_y, T_z	Engine thrust forces in the body axes	N
t	Time	s
V	Airspeed	m/s
α	Angle of attack	rad
β	Angle of sideslip	rad
ϕ, θ, Ψ	Aircraft bank, pitch and heading angle	rad
η, ξ, ζ	Elevator, aileron and rudder deflection	rad
ζ_V	Ventral rudder deflection	rad
σ	Standard deviation	-

Subscripts

0	Initial or trim value
LH, RH	Left hand, right hand
ref	Reference value

Superscripts

CG	Center of Gravity
NP	Neutral Point
RP	Aerodynamic moment reference point

Acronyms

AOA	Angle of Attack
AOS	Angle of Sideslip
ATRA	Advanced Technologies Research Aircraft
CFD	Computational Fluid Dynamics
CG	Center of Gravity
DLR	German Aerospace Center / Deutsches Zentrum für Luft- und Raumfahrt
FAA	Federal Aviation Administration
FTI	Flight Test Instrumentation
GUI	Graphical User Interface
IAS	Indicated Airspeed
MAC	Mean Aerodynamic Chord
N1	Engine low pressure shaft rotation speed
NP	Neutral Point, Aerodynamic Center
PID	Parameter Identification
RAPIT	Rapid Aerodynamic Parameter Identification Tool
SLD	Supercooled Large Droplets
Sys-ID	System-Identification
UDP	User Datagram Protocol

1. INTRODUCTION

Flight safety can be seriously affected by aircraft icing because the aerodynamic characteristics may change tremendously under icing conditions. As ice formations built up on the aircraft wing and the horizontal tail, aircraft performance as well as stability and control can be deteriorated [14]. A massive increase in drag along with a higher fuel consumption leads to a lower flight range. Ice on the aircraft wings results in flow separation at a lower angle of attack, thus the stall speed is higher than under clean aircraft condition. Ice formation on the horizontal tail reduces longitudinal stability and controllability because of a higher tendency for stall. In a same way, local flow separation on the wing can change abruptly aileron hinge moments, causing a loss in lateral control or results in an ice-induced roll upset. Especially aircraft with reversible flight controls are particularly threatened by this phenomenon.

The negative effects of inflight icing are responsible for a significant number of aircraft accidents [10]. Icing and its influence on aircraft stability and control is a long-term research subject [2, 23 - 25]. In order to train pilots how to operate an aircraft under icing conditions, accurate simulator models are needed [8, 25]. Certification authorities tackle the problem of aircraft icing by imposing rules on the manufacturers [18], where they have to show that the aircraft is tolerant to icing or is equipped with suitable ice protection systems. These systems must be designed in a way that they are able to detect icing conditions and activate ice protection systems to allow the aircraft to exit safely from areas with icing conditions. Icing envelopes have been developed, defining atmospheric conditions for the certification process. Nonetheless, in recent times it became apparent that aircraft icing may occur outside the defined envelope. As a result, the FAA updated their rules [17] on aircraft icing standards in October 2014 by adding new requirements which cover also icing caused by supercooled large droplets (SLD). SLDs are defined as water droplets greater than 50 microns. Even like smaller water droplets they are liquid below temperatures of 0°C and start to freeze when in contact with the cold aircraft surface. In difference to smaller water droplets, SLDs can dissolve or break up before freezing. Because of this splashing phenomenon, SLDs may form ice aggregations beyond the traditional ice protection systems.
A lack of research in understanding the SLD icing effects on aircraft and new certification rules were the starting point for a research initiative between the German Aerospace Center (DLR) and the Brazilian aircraft manufacturer EMBRAER. The main focuses of these investigations are the effects of SLD icing on the aircraft aerodynamics and developing certification strategies for future aircraft. EMBRAER provided a Phenom 300 prototype as test aircraft, while the DLR Institute of Flight Systems provided its expertise on system identification. One of the project goals was to develop a flight mechanical model which adequately reproduces the aircraft behavior under different icing conditions [5]. System identification flight tests were planned and performed for aerodynamic model development. This research effort was complemented by a joint research project between DLR and TU-Braunschweig called “SuLaDI” which among other icing topics has the aim to develop online parameter estimation algorithms which are able to provide information about the current aerodynamic characteristics.
Parameter estimation has been a valuable tool for the support of flight testing for a long time [20]. Accurate information about aerodynamic stability and control derivatives is needed to evaluate the handling characteristics of the aircraft and to design appropriate control laws. Methods permitting a quick comparison of the actual aircraft with the original design may speed up the certification process and increase flight test safety. Usually flight data are recorded onboard the aircraft and analyzed later on the ground because the system identification algorithms are computationally demanding. With increasing computing power and advanced data acquisition systems in the late 1990s, real-time estimation algorithms became practically usable onboard the aircraft. A sequential total least-squares method was applied in reference [13] to estimate aerodynamic parameters of a twin-engine turboprop aircraft. An extended Kalman filter was used to correct the sensor measurements for errors. In reference [27] the estimation of aerodynamic stability and control derivatives was demonstrated successfully on board a C-12C turboprop aircraft. Flight data were parsed automatically into time slices which were batch processed by a least-squares algorithm for the estimation of aerodynamic derivatives. Batch processing of flight test data was also used in reference [3] to develop a global nonlinear aerodynamic model onboard an Aermacchi MB-326M Impala jet aircraft. Two different types of aerodynamic models were investigated for in the online identification process: a fuzzy logic model and one consisting of multivariate orthogonal splines. In [15] aerodynamic stability and control derivatives of a subscale aircraft were successfully determined using Fourier transform regression which is another method for the online estimation of aerodynamic parameters. It works in the frequency domain and results are available in almost real time during the flight maneuver.

At the DLR Institute of Flight Systems two online parameter estimation tools were developed: RAPIT (Rapid Aerodynamic Parameter Identification Tool) and FITLAB-Online [4]. RAPIT works in the frequency domain and allows an estimation of aerodynamic stability and control derivatives in near real-time during the flight test maneuvers and compares them to reference values [21]. FITLAB-Online uses a Maximum Likelihood method [11] in the time domain for the estimation of aerodynamic derivatives. Flight maneuver data are automatically cut into time slices which are then batch processed for the estimation of aerodynamic parameters. Compared to the RAPIT method, the FITLAB-Online algorithm allows the parameter estimation of non-linear aerodynamic models valid for the whole flight envelope. Results are available within minutes after the maneuver and can already be analyzed during the debriefing after flight.

This paper shows the application of the two aforementioned tools to flight tests with an EMBRAER Phenom 300 aircraft equipped with artificial SLD ice shapes. The developed online parameter estimation tools were used to monitor the aerodynamic characteristics of the aircraft in flight and to quickly identify and evaluate the differences to the clean aircraft configuration which was analyzed by using existing flight test data. To the best of the authors’ knowledge this is the first time that the impact of SLD ice shapes on the aircraft aerodynamic characteristics are analyzed in both longitudinal and lateral direction in near real-time during flight test.

In chapter 2, the two online analysis tools are introduced and the estimation methods are explained briefly. The flight test setup and the performed maneuvers are explained in chapter 3. Results from the online evaluation of the flight test data are presented in chapter 4. This includes also a comparison of aerodynamic model parameters determined from the flights with SLD icing shapes with the ones determined from flights with the clean aircraft. Finally a conclusion and an outlook on future research activities are given in chapter 5.

2. ONLINE ANALYSIS TOOLS

2.1. RAPIT

RAPIT is based on a parameter estimation method called ‘Fourier transform regression’ being explained briefly in the following sections. RAPIT already demonstrated a successful estimation of aerodynamic parameters during a flight test campaign with the DLR research aircraft ATRA

[22]. Here the software tool was installed onboard an Airbus A320 and system identification maneuvers were performed.

2.1.1. Total Aerodynamic Coefficients

The first step in the estimation process is the determination of the total aerodynamic force and moment coefficients. They are calculated from the measured translational accelerations at the aircraft CG and the angular rate measurements. Engine thrust and moments, calculated using an engine model, are subtracted from the total forces and moments to determine the aerodynamic ones. Eqs. (1) to (3) describe the calculation of the aerodynamic force coefficients in the aircraft body-fixed axes.

(1) $$C_X = (ma_x^{CG} - T_x)/(\bar{q}S)$$

(2) $$C_Y = \left(ma_y^{CG} - T_y\right)/(\bar{q}S)$$

(3) $$C_Z = (ma_z^{CG} - T_z)/(\bar{q}S)$$

S is the wing area, $\bar{q}$ the measured dynamic pressure, $a_x^{CG}, a_y^{CG}, a_z^{CG}$ are the measured linear accelerations at the aircraft CG and T_x, T_y, T_z are the engine force components in body-fixed axes. The lift and drag coefficients result from rotating the force coefficient around the angle of attack α

(4) $$C_L = -C_Z \cos\alpha + C_X \sin\alpha$$

(5) $$C_D = -C_X \cos\alpha - C_Z \sin\alpha$$

The aerodynamic moment coefficients $C_l^{CG}, C_m^{CG}, C_n^{CG}$ in body-fixed axes are computed from the angular rates p, q, r, rotational accelerations $\dot{p}, \dot{q}, \dot{r}$, moments of inertia $I_{xx}, I_{yy} I_{zz}, I_{xz}$, and the engine moment components at the aircraft center of gravity $M_x^{CG}, M_y^{CG}, M_z^{CG}$. The necessary rotational accelerations are obtained by numerical differentiation of the angular rates in the frequency domain.

(6) $$C_l^{CG} = \frac{1}{\bar{q}Ss} \cdot \left[I_{xx}\dot{p} - I_{xz}(pq + \dot{r}) + \left(I_{zz} - I_{yy}\right)qr - M_x^{CG}\right]$$

(7) $$C_m^{CG} = \frac{1}{\bar{q}Sl_\mu} \cdot \left[I_{yy}\dot{q} + (I_{xx} - I_{zz})pr + I_{xz}(p^2 - r^2) - M_y^{CG}\right]$$

(8) $$C_n^{CG} = \frac{1}{\bar{q}Ss} \cdot \left[I_{zz}\dot{r} + I_{xz}(\dot{p} - qr) + \left(I_{yy} - I_{xx}\right)pq - M_z^{CG}\right]$$

Equations (6) to (8) determine the aerodynamic moment coefficients at the aircraft CG. Using the lever arms between a geometrically fixed point and the current location of the aircraft CG, the moment coefficients are transformed to a common body-fixed reference point RP at 25 % MAC. This processing step is necessary to make the later estimated moment derivatives comparable to results from flight tests with the clean aircraft configuration. The total aerodynamic force and moment coefficients presented in the Eqs. (1) to (8) are evaluated each time new measurements from the aircraft sensors are available.

2.1.2. Aerodynamic Derivative Model

A set of six linear equations for the total force and moment coefficients defines the aerodynamic model. Each equation consists of a summation of a bias term and of derivative terms describing different influences on the particular aerodynamic force or moment. The model equations approximate the total aerodynamic force and moment coefficients derived from measurements with the Eqs. (1) to (8). The aim of the subsequent parameter estimation process is to determine the derivative terms in the model equations so that the aerodynamic coefficients, derived from measurements, matches the result of model outputs. Eqs. (9) to (11) determine the total force and moment coefficients for the longitudinal aircraft motion. They are functions of the angle of attack α, pitch rate q, elevator deflection η, and the average spoiler deflection sp_{avg}:

(9) $$C_L = C_{L0} + C_{L\alpha}\alpha + C_{Lq}\frac{ql_\mu}{V} + C_{L\eta}\eta + C_{Lsp}\, sp_{avg}$$

(10) $$C_D = C_{D0} + C_{D\alpha}\alpha + C_{Dq}\frac{ql_\mu}{V} + C_{D\eta}\eta + C_{Dsp}\, sp_{avg}$$

(11) $$C_m^{RP} = C_{m0} + C_{m\alpha}\alpha + C_{mq}\frac{ql_\mu}{V} + C_{m\eta}\eta + C_{msp}\, sp_{avg}$$

The equations approximate the lift, drag and pitch moment coefficients derived from measurements with Eqs. (4), (5), and (7). Similarly, the coefficients for the lateral motion, as described in Eqs. (12) to (14), are functions of the angle of sideslip β, roll rate p, yaw rate r, aileron deflection ξ, rudder deflection ζ, asymmetric spoiler deflection sp_{diff} and ventral rudder deflection ζ_V. Spoiler deflections show up in the equations for the longitudinal as well as the lateral aircraft motion. They are used as speed brakes or support roll maneuvering. The average spoiler deflection is the mean of the LH (left hand) and RH (right hand) spoiler deflections, whereas the asymmetric spoiler defection is determined from the difference of the LH and RH spoiler deflections. The equations for the lateral motion approximate the side force, roll and yaw moment coefficients derived from measurements with Eqs. (2), (6), and (8).

(12) $$C_Y = C_{Y0} + C_{Y\beta}\beta + C_{Yp}\frac{ps}{V} + C_{Yr}\frac{rs}{V} + C_{Y\xi}\xi + C_{Y\zeta}\zeta + C_{Y\zeta_V}\zeta_V + C_{Ysp}sp_{diff}$$

(13) $$C_l^{RP} = C_{l0} + C_{l\beta}\beta + C_{lp}\frac{ps}{V} + C_{lr}\frac{rs}{V} + C_{l\xi}\xi + C_{l\zeta}\zeta + C_{l\zeta_V}\zeta_V + C_{lsp}sp_{diff}$$

(14) $$C_n^{RP} = C_{n0} + C_{n\beta}\beta + C_{np}\frac{ps}{V} + C_{nr}\frac{rs}{V} + C_{n\xi}\xi + C_{n\zeta}\zeta + C_{n\zeta_V}\zeta_V + C_{nsp}sp_{diff}$$

Each derivative term in Eqs. (9) to (14) has a dedicated influence on the static and dynamic characteristics of the aircraft [9]. For example, values for the lift curve slope $C_{L\alpha}$ and the pitching moment derivative $C_{m\alpha}$ define the aircraft's static stability margin. Other important properties are control derivatives like e.g. the aileron effectiveness $C_{l\xi}$ and the yaw damping C_{nr}.

2.1.3. Fourier Transform Regression

The equations in section 2.1.2 can be stated for each new measurement that is acquired. Written in matrix form, they lead to an overdetermined system of equations. This system of equations constitutes a linear regression problem: On the left side are the aerodynamic coefficients being determined from the acceleration and angular rate measurements Eqs. (1-8), on the right side are the modeled aerodynamic derivatives being multiplied by measured flight mechanical quantities and control deflections Eqs. (9-14). The derivatives in Eqs. (9-14) have to be determined in a way that the model results in a 'best fit' for the calculated aerodynamic coefficients. This parameter estimation problem can be solved by equation error methods. The challenge of online parameter estimation is however, that both sides of the equation are updated each time new measurements are acquired.

One suitable method for online parameter estimation is Fourier transform regression which is implemented in the RAPIT software. It was developed by Morelli [13, 12] and solves the equation error problem in the frequency domain. For this purpose the aerodynamic coefficients determined with Eqs. (1-8) and the flight mechanical measurements $(\alpha, \beta, p, q, r, V)$ as well as the control deflections $(\eta, \xi, \zeta, sp_{avg}, sp_{diff})$ on the right side are Fourier transformed. This transformation is done with a recursive algorithm which is applied to the left-hand and right-hand terms each time the regression equations are updated. Working in the frequency domain has the advantage of having a fixed memory size for data operations, because only the Fourier transformed values at the specified frequencies need to be updated and stored. The algorithm allows limiting the evaluation of the Fourier transformation to the frequency range of interest. For flight tests with the Phenom 300 the Fourier transformation was evaluated for a frequency band from 0.05 to 2 Hz with intervals of 0.01 Hz. Flight data were obtained at a rate of 11.4 Hz. Discarding all frequencies smaller than 0.05 Hz after the Fourier transformation removes also bias and drift in the measured values. As a consequence it is not possible to estimate the trim or zero coefficients in the aerodynamic model. However, the missing aerodynamic zero coefficients are of minor concern for the flight test, because these terms do not affect the task of monitoring the aircraft's control and stability characteristics. A least-squares solution is computed for each transformed regression equation (Eqs. (9) - (14)) and the aerodynamic derivatives are estimated. For each estimated parameter the standard deviation σ is calculated from the covariance matrix of the least-squares solution as described in references [10] and [12]. Least-squares estimation is repeated at fixed time intervals using the Fourier transformed regression equations. During the performed flight tests, estimates for the aerodynamic derivatives were updated every second.

2.1.4. Operation and User Interface

RAPIT is an online parameter estimation tool implemented with the software development environment LabVIEW. It was designed to run on a laptop equipped with a dual core 2.90 GHz processor and 8 GB RAM under MS Windows 7. A graphical user interface allows easy operation of the software. The parameter estimation process is started and stopped by the user to optimally cover the flight maneuvers of interest. RAPIT is connected to a MySQL database which contains

- software setup values,
- reference values for each aerodynamic derivative which in this case were the results from flight tests with the clean aircraft configuration,
- all aerodynamic derivatives determined during each parameter estimation run.

As the database contains all results from different test points, it is possible to compare the estimated aerodynamic derivatives during the flight test. This feature was used e. g. to monitor the aileron effectiveness with decreasing air speed as mentioned in section 3.3. The database can be accessed by other software tools like MS Excel, permitting a more in-depth analysis of the results on ground. Tabs on the graphical user interface allow the selection of different data views. The user can observe the execution of flight tests by taking a look at time series plots of the

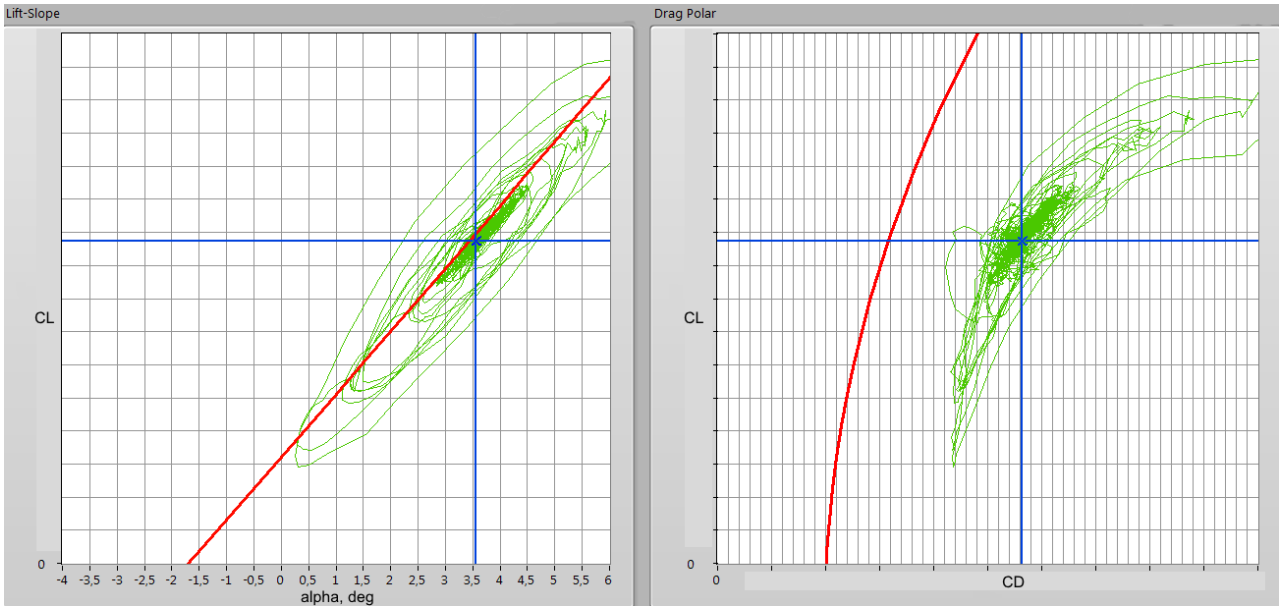

Figure 1: Lift curve and drag polar during flight with artificial ice shapes. Current values (blue crosses), test point maneuver history (green) and clean aircraft model reference (red).

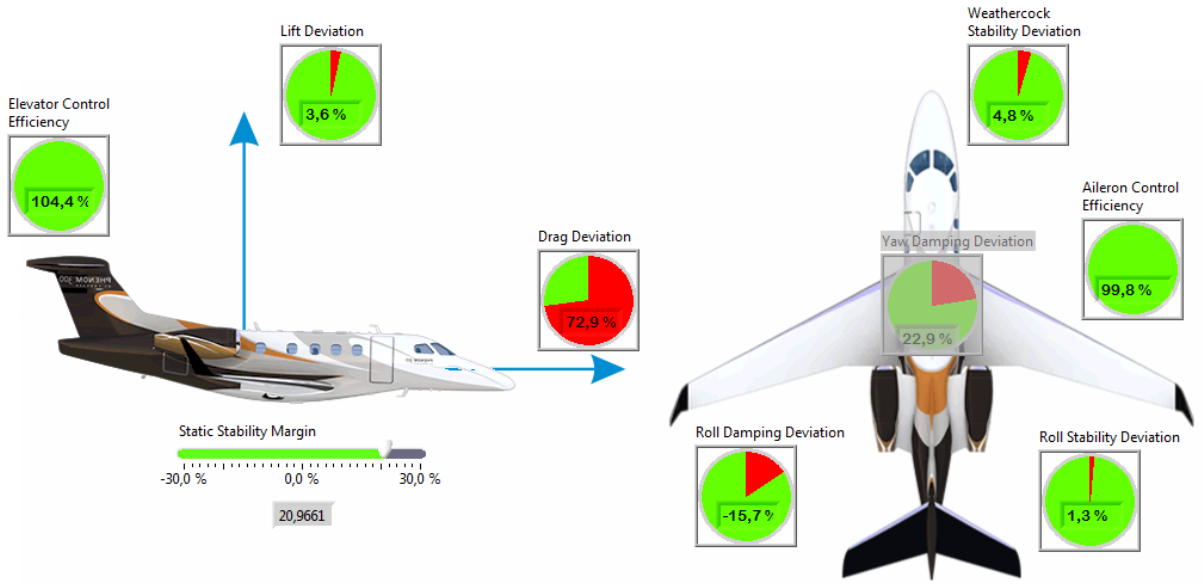

Figure 2: Aircraft stability and control monitor view.

measured sensor data. A tabular view lists all derivatives used in Eqs. (9) to (14) with their estimated value and the standard deviation which is updated each time a new least squares estimated has been executed.
Quick looks of the estimation results assist the flight test engineer in evaluating the maneuver quality and support him on the decision of how to proceed with the flight test program. Total lift and drag coefficients C_L and C_D are continuously computed according to Eqs. (4) and (5) because they are required for the parameter estimation process. These values are compared in real-time to an aircraft performance model determined from flight data with the clean aircraft configuration. Figure 1 shows a data view with this comparison during a flight with artificial ice shapes: Current values for the lift and drag state of the aircraft are marked by blue crosses. Model predictions for the lift curve and the drag polar of the clean aircraft are represented by the red lines. Green lines mark the time history of the actual lift and drag coefficients recorded during maneuvers at the current test point. Differences in the performance between clean and iced aircraft configuration are quickly identified using these two graphs and the lift situation near high angle of attack can be monitored. During flight test, awareness of the current aircraft stability and control state is important for the flight crew, because a significant degradation may lead to an unsafe situation. The data view shown in Figure 2 shows information about the current aerodynamic characteristics and the deviation from the clean aircraft configuration as reference. Dial gauges - similar to engine indications - represent values for a comparison of the main aircraft stability and control characteristics. For the stability and damping terms the difference between the reference and the estimated value is shown as percentage in numbers and also graphically as a red surface on the green dial. Concerning the control efficiency indications for elevator and aileron, a value of 100 % means that the estimated control derivative equals the value for the clean aircraft as reference. If the estimated value is smaller than the reference, the loss is shown as a red surface. Another important indicator is the static stability margin which is the relative distance between the CG and the aerodynamic neutral point NP. For a statically stable aircraft the location of the CG must be forward of the NP so that the static margin should always be positive. The current static margin is indicated on a measuring scale below the aircraft drawing. Visibility of the stability and control indications is controlled by a limit for the standard deviation of the estimated aerodynamic derivatives. The indication is greyed out for values of the standard deviation greater than 6 %. In Figure 2 this is the case for the yaw damping deviation.

2.2. FITLAB-Online

The second herein presented online parameter estimation tool is able to estimate parameters of an arbitrarily complex nonlinear 6-DOF aircraft simulation model in time domain. These models are usually used in simulators or for flight dynamics evaluation and are able to cover the complete flight envelope. By comparing the measured and simulated outputs the estimation method guarantees, that the resulting model behavior is comparable to the real aircraft. The tool uses an adapted version of the DLR parameter estimation software FITLAB [26] and has several extensions to allow the online capability. An overview of the online estimation tool [4] is given in Figure 3. It contains several individual parts used to receive, search and preprocess data as well as estimating the requested model parameters.

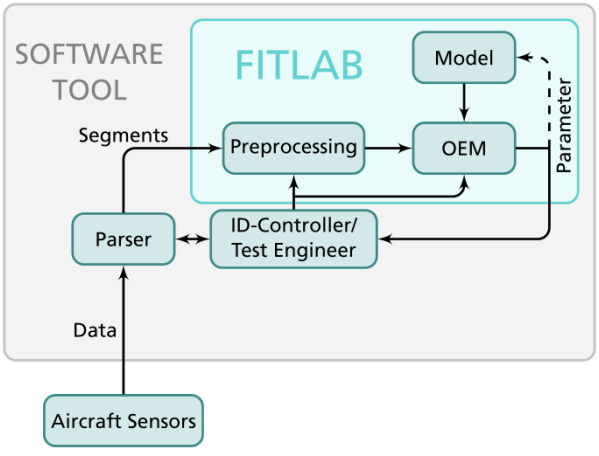

Figure 3: Tool chain of time domain online parameter estimation.

In the following, the different software parts are explained:

Data acquisition and transfer: Flight data are received via UDP and stored in a shared memory allowing access to each part of the software.

Data Parser: The stored flight data are searched by a parser algorithm. It browses the collected flight data for maneuvers being useful for parameter estimation and marks the detected segments with indication of start and end time.

Preprocessing: Unit conversions in order to match the measured flight data with the inputs expected by the flight mechanic model is done in a preprocessing step.

Output Error Method (OEM) and Simulation Model: The Output Error Method conventionally used for time domain parameter estimation applications is implemented in FITLAB and described in detail in several publications such as [11]. Arbitrary nonlinear complex simulation models can be used with the FITLAB core. For the current implementation, a model formulation representing the aircrafts longitudinal motion under icing conditions is used and briefly described in section 2.2.1 as well as in reference [7].

2.2.1. Aerodynamic Model

The FITLAB-Online parameter estimation application for the Phenom 300 SLD icing flight tests uses the same aerodynamic model approach as presented in [7]. Therefore a basic aircraft model using clean configuration flight test data was developed prior to the icing flight tests. For covering the aerodynamic icing effects a Δ-model was formulated which can be added when required (see Figure 4). The forces and moments determined by the aerodynamic model are used in the equations of motion of a flight mechanical model. Outputs from this model like accelerations, angular rates, Euler angles, AOA and AOS are approximated to measurements from flight test maneuvers by estimating the aerodynamic parameters. For the icing flight tests the objective was mainly to estimate the longitudinal Δ-model parameters and keeping the base model fixed. For example the condensed Δ-model for drag used in the flight test is given by the following equations:

$$\Delta C_{D\,\mathrm{Ice}} = k_{CD0} \cdot C_{D0\,\mathrm{Base}} + C_{L\,\mathrm{Base}} \cdot d_{k1} + (C_{L\,\mathrm{Base}})^2 \cdot \frac{d_{k2}}{e\Lambda\pi} + \Delta\hat{X}_{\mathrm{Ice}}(k_{\alpha^*}) \left(\frac{\partial C_D}{\partial \hat{X}}\right)_{\mathrm{Base}} \tag{15}$$

The change of the non-dimensional flow separation point given by

$$\Delta\hat{X}_{\mathrm{Ice}}(k_{\alpha^*}) = \frac{\tanh(a_{1\mathrm{Ice}}) - \tanh^2(a_{1\mathrm{Base}})\tanh(a_{1\mathrm{Ice}})}{-2(1 + \tanh(a_{1\mathrm{Base}})\tanh(a_{1\mathrm{Ice}}))} \tag{16}$$

with the auxiliary variables

$$a_{1\mathrm{Ice}} = -c_{1\mathrm{Base}}\,\alpha^*\,k_{\alpha^*} \tag{17}$$

$$a_{1\mathrm{Base}} = c_{1\mathrm{Base}}\,(\alpha - \alpha^*)$$

containing the influence of the angle of attack via the parameter α^*, allows to change the aircraft stall point due to the icing effects. A further detailed derivation of these equations is outlined in [7]. Concerning the Eqs. (15) to (17) of the aerodynamic Δ-model this results in 4 additional parameters k_{CD0}, d_{k1}, d_{k2} and k_{α^*} ,being determined with the online system identification algorithm.

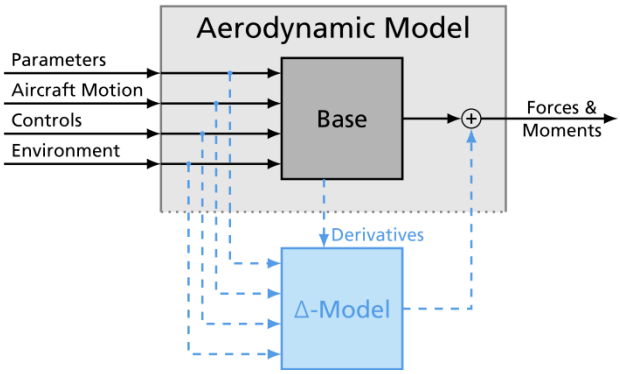

Figure 4: Illustration of aerodynamic model with Δ-model extension.

To cover changes in the lateral dynamics, several parameters of a decoupled lateral motion model were estimated and compared the base model parameter values.

2.2.2. User Interface

The main user interfaces for the time domain parameter estimation during flight test consist of two GUIs. The data parser GUI is shown and explained in Figure 5.

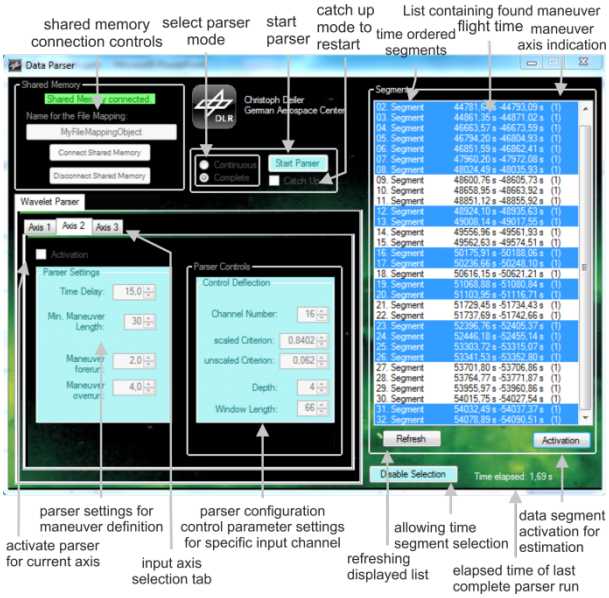

Figure 5: GUI flight data parser.

After connecting to the flight data shared memory, the parser can be configured by selecting a search data channel; certain settings and controls for detecting elevator, aileron and rudder step inputs are predefined [6]. Automatically found segments are continuously listed on the right table of the GUI window. They can be activated for

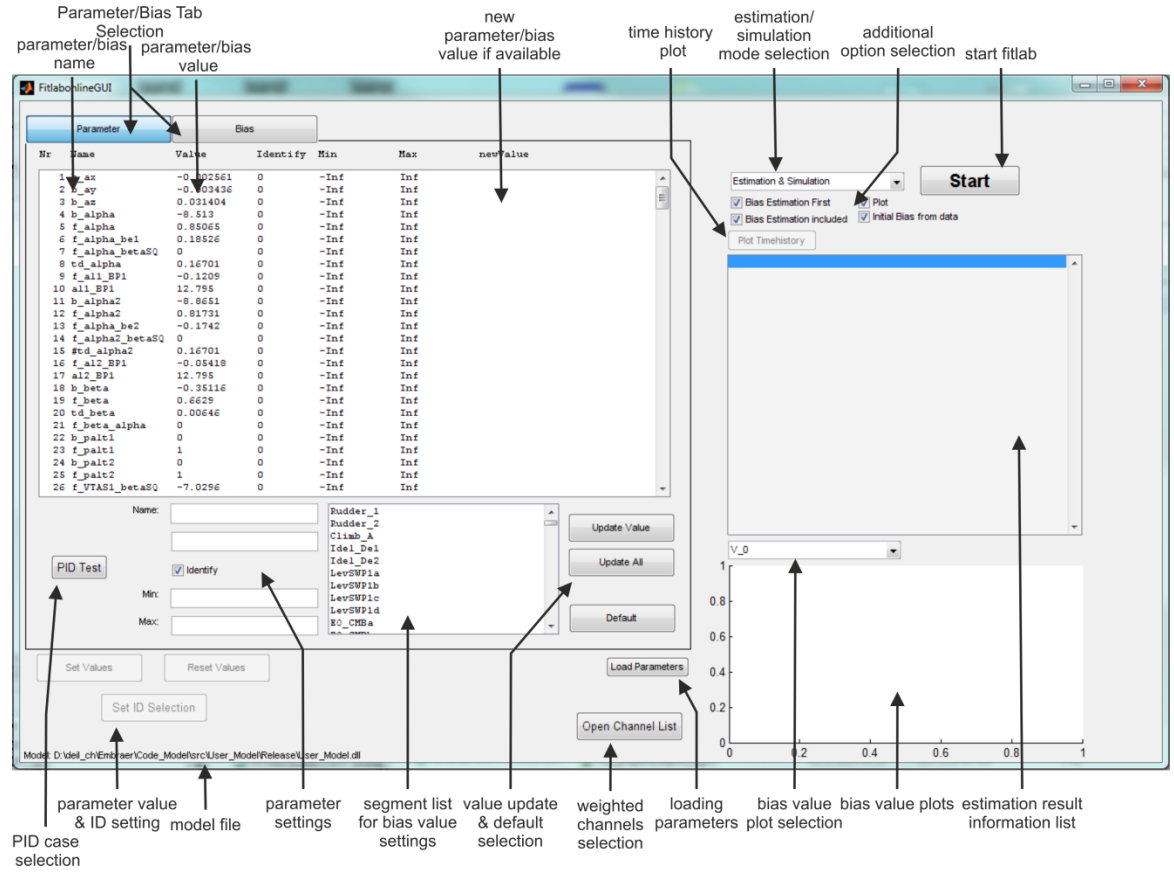

Figure 6: FITLAB-Online GUI for controlling the parameter estimation process and plotting the results.

estimation by pressing the “Activation” button.

The second GUI running in parallel for controlling FITLAB-Online is shown in Figure 6. This interface combines all required parts for parameter estimation, which are the

- selection of free and fixed parameters,
- control of parameter and/or bias updating,
- estimation / simulation start and
- plotting of parameter estimation results.

The annotations in Figure 6 explain the different parts of the GUI and show how to control the software for running an essential parameter estimation task.

3. FLIGHT TEST

3.1. Test Aircraft

Figure 7: EMBRAER Phenom 300 test aircraft.

EMBRAER provided a prototype of the Phenom 300 business jet as test aircraft depicted in Figure 7. It is a twin engine aircraft with a horizontal stabilizer in T-tail configuration. The Phenom 300 has a MTOW of 8.3 t and a wingspan of 16 m. It is equipped with a conventional reversible flight control system. The anti-ice systems include leading edges of the wings and horizontal tail as well as the engine intakes. For the flight tests artificial ice shapes made of plastic material were glued to the aircraft skin. Figure 8 shows these shapes on the wing upper and lower surface. Four different aircraft configurations were flown during the flight test program:

1) Clean: The aircraft without any modifications.
2) Low-Risk SLD: Artificial ice on the radome, winglets and on the wing upper and lower surface without the wing area of the ailerons (SLD I).
3) Incremental SLD: Artificial ice on the radome, winglets and on the wing upper and lower surface including the wing area of the ailerons (SLD II).
4) Nominal SLD: Artificial ice on the radome, engine pylons, winglets and on the wing upper and lower surface including the wing area of the ailerons (SLD III).

Flight tests with the clean aircraft were performed end of 2014, whereas tests with the artificial ice configurations were performed end of 2015. The aircraft was equipped with standard air data sensors and an inertial reference platform. Flight data could be processed onboard with a laptop connected to an onboard flight data network. During flight tests with the clean aircraft the flight crew consisted of two pilots, two flight test engineers and one experimental engineer. Flight data could also be sent to a telemetry station on ground. The telemetry was used during all flights with artificial ice shapes because they were classi-

fied as high risk flights and only a minimum crew of two pilots and one flight test engineer was allowed only.

Figure 8: Artificial shapes for SLD icing on the upper and lower wing surface, outer wing and radome.

3.2. Flight Test Setup

A prerequisite for the online processing of flight data was the creation of a suitable interface to the existing flight data acquisition environment of EMBRAER. Figure 9 shows an overview of the software setup that was used during the flight test trials. All data measured by the aircraft sensors and signals from the different aircraft systems were acquired by a central telemetry server. The telemetry server provided a continuous data stream with a sample rate of 88 ms which could be accessed by a communication interface. Two laptops running the online analysis tools were connected to the server by a standard Ethernet network cable. Pre-processing was necessary before the flight data could be used by the online estimation tools. For this task a “Flight Data Client” was programmed which was executed on one of the laptops connected to the telemetry server. The client acquired selected measurements from various sensors e. g. air data system, inertial reference platform and engine rotational speed. If necessary, measurements were corrected with calibration equations determined from a data compatibility check with former flight data. For the determination of the total aerodynamic coefficients, engine forces and moments were required. These were computed by an engine model using engine rotation speed N1, Mach number and pressure altitude as input. A weight and balance routine calculated the current aircraft weight, CG position and moments of inertia. Aircraft ramp weight and CG position as well as the current fuel content were needed for this calculation. The flight data client gathered the calculated data as well as the sensor measurements and sends it to RAPIT and FITLAB-Online using a multicast UDP. It was possible to install the described software setup on ground in a telemetry room as well as directly onboard the aircraft. That way, the online analysis tools could also be operated by a flight test engineer in the aircraft during flight, in cases the telemetry data connection to ground was not available.

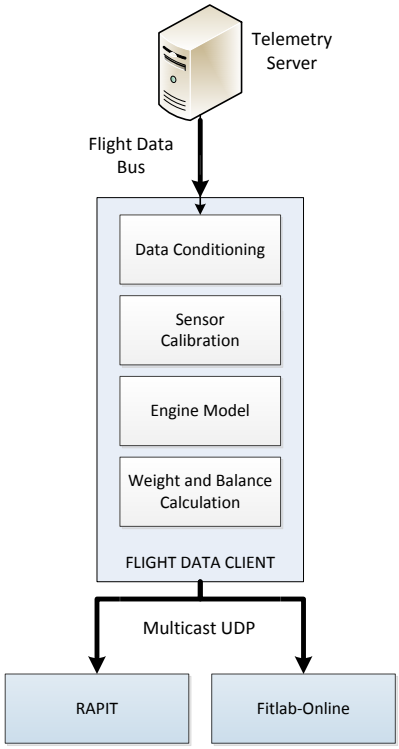

Figure 9: Schematic overview of the online analysis tools software setup.

3.3. Flight Test Program

System-Identification maneuvers were performed at three different altitudes and two different velocities according to the test point definitions listed in Table 1, in order to investigate the aircraft handling characteristics and its performance. The maneuvers consisted of the following step inputs into the aircraft control surfaces:

- Elevator-3211.
- Single elevator step input to excite the phugoid motion.
- Bank-to-bank maneuver with ailerons and activated roll spoilers.
- Bank-to-bank maneuver only with ailerons.
- Ruder doublet maneuver with ventral rudder damping.
- Rudder doublets maneuver without ventral rudder damping.

All maneuvers started from a trimmed horizontal flight condition specified by the test point definition. The low speed limit of 170 kt V_{IAS} was established after analyzing wind tunnel experiments, which resulted in an increase of the stall speed by a factor of nearly 1.3 for configurations with artificial ice shapes. Monitoring of the aileron effectiveness was critical during flights with artificial ice shapes. For this reason a special maneuver was performed prior to the typical System-Identification maneuvers. The aircraft was accelerated to 210 kt V_{IAS} and bank-to-bank maneuvers with low amplitudes were performed. RAPIT was used to estimate the aileron control effectiveness derivative. After a successful estimation process the aircraft decelerated by 10 kt and the bank-to-bank maneuver was repeated. The estimated aileron control effectiveness was monitored and the procedure was repeated until the aircraft reached a velocity of 170 kt.

No.	V_{IAS}	Altitude
1	170 kt	10000 ft
2	220 kt	10000 ft
3	170 kt	15000 ft
4	220 kt	15000 ft
5	170 kt	20000 ft
6	220 kt	20000 ft

Table 1: Test points for flights with artificial ice shapes.

4. RESULTS AND DISCUSSION

4.1. RAPIT

4.1.1. Lift-Drag Situation

Right after take-off the aircraft lift and drag status was closely monitored using the scopes depicted in Figure 1 and Figure 2. Before the initiation of the flight maneuvers, the aircraft approached a stationary state with constant altitude and velocity. The determined total lift and drag coefficients at this trimmed condition were compared to an aerodynamic model identified from flight tests with the clean aircraft, considering the same AOA, Mach number and stabilizer trim. The results of this comparison are listed in Table 2.

	AOA, deg	C_L Dev. f. Clean, %	C_D Dev. f. Clean, %
SLD I	3.5	-1.8	57.3
SLD II	3.5	-2.9	71.7
SLD III	3.6	-3.2	73.0

Table 2: Measured lift and drag deviations from the clean aircraft at 15000 ft and 170 kt V_{IAS}.

Lift and drag coefficients were determined at a trimmed flight condition of 15000 ft altitude and 170 kt V_{IAS} and then averaged over 25 measurements. The artificial SLD ice shapes significantly increased the total aircraft drag. The 'Low-Risk' configuration SLD I showed already a drag increment of nearly 60 % compared to the clean aircraft. This resulted also in higher fuel consumption, cutting the available flight test time by 50 %. Covering the wing outer area near the ailerons with the ice shapes in configuration SLD II increased the drag further to over 70 %. Ice shapes on the engine pylons as in configuration SLD III raised the drag further by additional 1.3 %. A comparison of the total lift coefficients showed no significant difference to the clean aircraft situation. The lift is nearly 2 % less in configuration SLD I and over 3 % less in configuration SLD III. Although the lift characteristics showed no major deterioration, the deviation from the linear region must be observed in more detail for lower speeds i.e. higher angles of attack. On the current flights, however the lowest speed was limited to 170 kt V_{IAS} for safety reasons.

4.1.2. Aileron Effectiveness

Monitoring of the lateral controllability was of particular interest for the flight test crew because wind tunnel experiments with the SLD ice shapes showed flow separation on the outboard wing area near the ailerons at high angles of attack. For this reason, first a low risk configuration (SLD I) with no ice shapes in front of the ailerons was flown and then a configuration (SLD II) with the wings fully equipped with shapes. As already mentioned in section 3.3, at the start of each test program short aileron step inputs with decreasing airspeed were flown to check the aileron effectiveness with RAPIT. Time series plots in Figure 10 show the results determined with RAPIT during one aileron step excitation with the SLD I configuration.

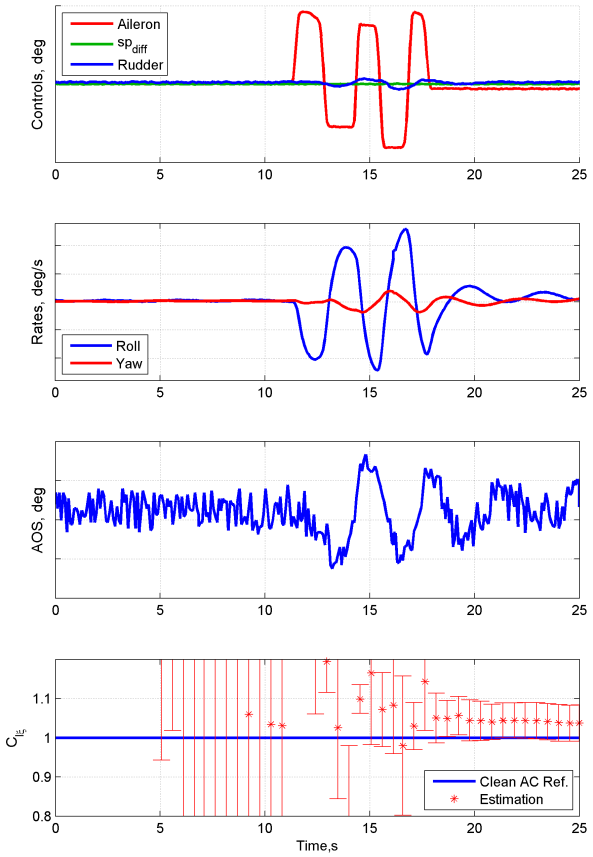

Figure 10: Online estimation of the aileron efficiency $C_{l\xi}$ with RAPIT during an aileron step input.

The first graph shows the control surface deflections of aileron, rudder and roll spoilers, the second graph the roll and yaw rate and the third one the angle of sideslip during

the maneuver. In the last graph the progress of the estimation of the aileron control derivative $C_{l\xi}$ is shown. Red stars mark the estimated aileron control derivative at each time point. Error bars around the estimates indicate a 95 % interval calculated from the standard deviation. All estimates are normalized to a reference value determined from tests with the clean aircraft. An estimate with a value of one equals the reference being marked with a blue line. The estimation algorithm started processing flight data five seconds before the first estimation. Then a least-squares estimation was conducted every second as can be seen from the plot. The algorithm only used the measurements acquired during the maneuver and had no a-priori information about the derivative. Before the maneuver the estimated values were far off the reference line. After the maneuver the estimates converged towards a constant value, close to the reference line. In this case the estimated $C_{l\xi}$ was slightly higher than in the clean aircraft configuration, which cannot be explained in detail.

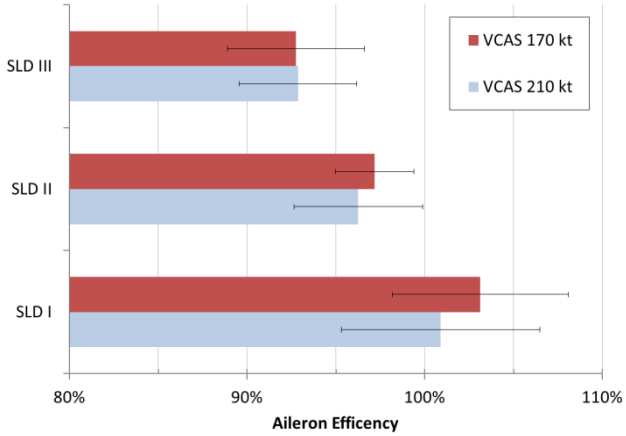

Figure 11: Estimated aileron control efficiency at different airspeeds and for different SLD configurations.

Figure 11 shows the results of the estimated aileron derivative for different SLD configurations. The values were again normalized with the derivative using the clean aircraft as reference. For each SLD configuration the estimated derivative is shown for 170 and 210 kt V_{IAS}. The error indicator marks the 95 % interval for the estimated value, calculated from the standard deviation. Taking a look at the bars the following tendency can be seen: All configurations were the wings were fully covered with the ice shapes showed lower aileron effectiveness. It decreased to nearly 93 % in the SLD III configuration. In general the results show that the deterioration of the aileron effectiveness is not very pronounced. The differences between the estimates for airspeed of 170 kt and 210 kt are also not very significant. The confidence intervals are much larger than the differences between the SLD configurations. For that reason the online estimation can only give a tendency which has to be examined further with advanced algorithms like described in section 4.2.2. During the tests at different airspeeds the AOA ranged only from 1.8 to 3.8 deg, at higher AOA the control degradation may become larger. However RAPIT confirmed within seconds after the maneuvers the results from wind tunnel tests which also showed a degradation of 7 % in aileron effectiveness [19].

4.1.3. Influence on Yaw Stability

The massive gain in drag on the aircraft wings affects the lateral stability derivatives, especially those concerning the yaw axis. In order to identify changes in the yaw stability several bank-to-bank, rudder doublet and steady heading sideslip maneuvers were performed at the test points. In Table 3 yaw stability derivatives are listed, estimated by RAPIT directly after these maneuvers with configuration SLD III. The results show that the weathercock stability derivative $C_{n\beta}$ has increased moderately by 6.7 %. A relative error of only 2.2 % indicates a good quality for this estimate. More noticeable are the changes in the yaw damping derivative C_{nr} which has increased due to the ice shapes by nearly 50 % compared to the value of the clean aircraft. The roll-yaw coupling derivative C_{np} also changed significantly by decreasing more than 60 %. However both estimates show large relative errors of nearly 26 % for C_{np} and 10 % for C_{nr}. One reason for the poor quality of the estimates could be that the linear model is not able cover all the nonlinear effects of the ice shapes on the lateral stability. The influence of the SLD ice shapes on yaw stability are analyzed in more detail in section 4.2.2, using the maximum likelihood algorithm on the total flight data acquired during each flight.

Derivative	Rel. Error, %	Δ from Clean, %
$C_{n\beta}$	2.2	6.7
C_{np}	25.5	-60.8
C_{nr}	9.5	47.6%

Table 3: Estimated yaw stability derivatives for configuration SLD III and their deviation from the clean aircraft configuration.

4.2. FITLAB-Online

During flight test FITLAB-Online was mainly used for monitoring the lift and drag characteristics of the aircraft with different artificial ice shape installations (see section 3.1). The data parser worked well and nearly all relevant time slices with Sys-ID maneuvers in longitudinal as well as in lateral motion were detected and marked automatically. After finishing all maneuvers a complete evaluation for the longitudinal motion was performed quickly. Lift curves and drag polars for the actual icing case in comparison to the clean aircraft case could be discussed with the overall flight test team already in the flight debriefing. First lateral motion evaluations were performed directly afterwards so that a comprehensive view of the aircraft characteristics under the tested ice shapes was available shortly after touchdown.

4.2.1. Lift-Drag Situation

Figure 12 to Figure 17 show some FITLAB-Online results for longitudinal motion. The time history plots (Figure 12 and Figure 14) show exemplary three elevator-3211 inputs and have the same color scheme as the lift curve slopes and drag polars. The blue lines show the measured flight test data, the black dashed lines show the clean aircraft simulation model and the red lines show the newly identified icing models. Figure 12 and Figure 13 illustrate the results for the SLD I icing case. Due to flight safety reasons the pilots handled the aircaft very carefully especially during the first SLD flight (AOA range from 0 to

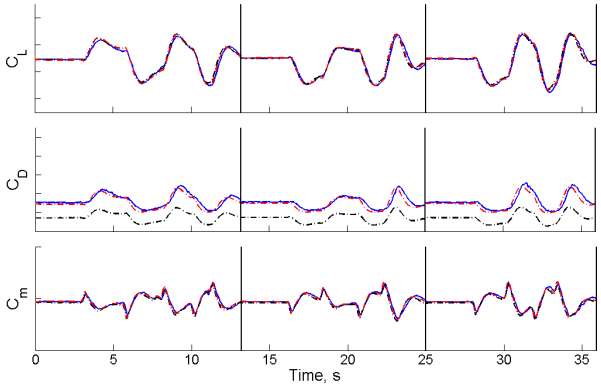

Figure 12: SLD I time histories of long. aerodynamic coefficients for elevator-3211 multistep input maneuvers (blue: flight test measurement / black: model clean / red: identified icing model).

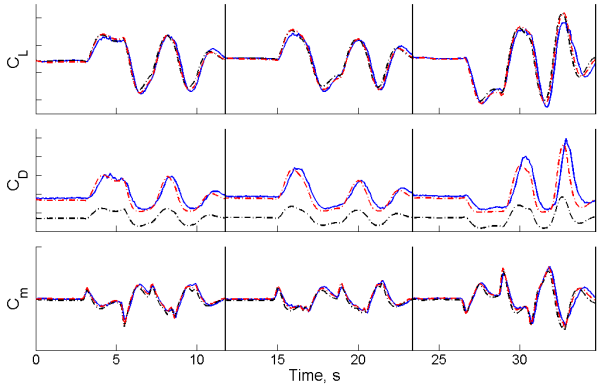

Figure 14: SLD III time histories of long. aerodynamic coefficients for elevator-3211 multistep input maneuvers (blue: flight test measurement / black: model clean / red: identified icing model).

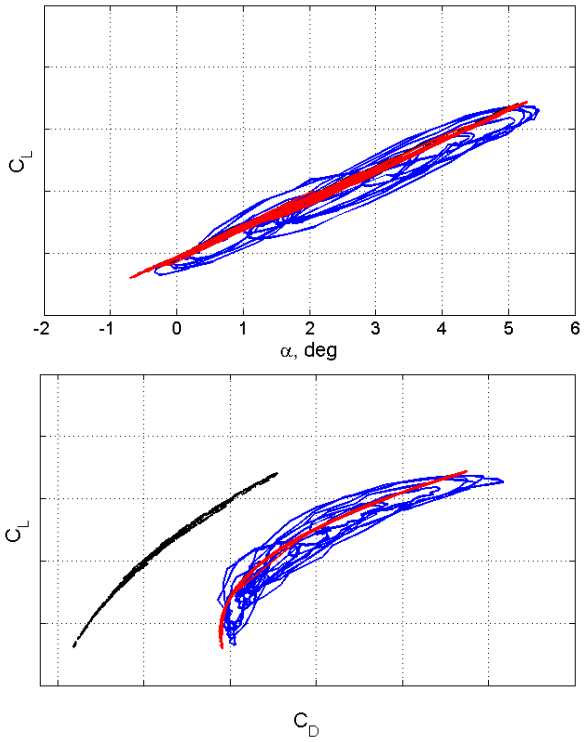

Figure 13: SLD I lift curve and drag polar (blue: flight test measurement / black: model clean / red: identified icing model).

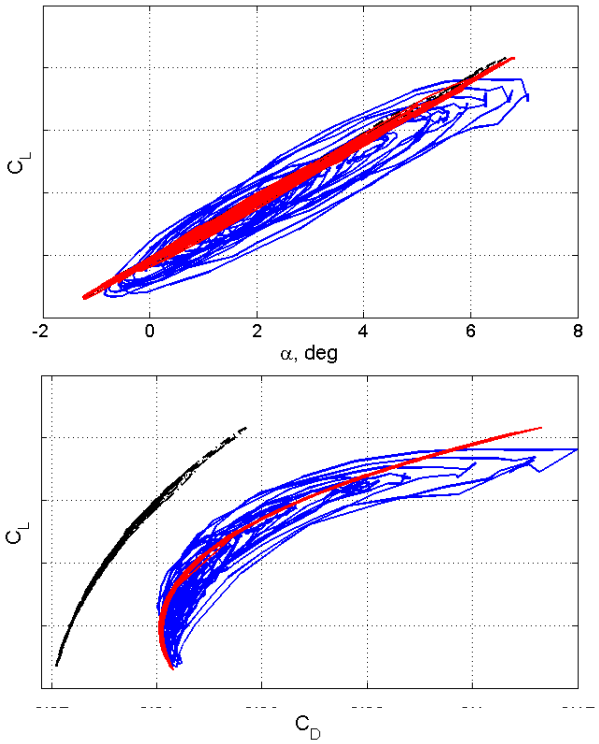

Figure 15: SLD III lift curve and drag polar (blue: flight test measurement / black: model clean / red: identified icing model).

5 deg). It can be seen clearly that the aircraft has operated only in the linear region of the lift curve and no measureable nonlinear lift curve slope change compared to the clean aircraft was observed. The drag polar has changed drastically and shows a drag at zero lift increase of about 100% compared to the clean aircraft case. The estimated drag parameter values of the icing Δ-model (see section 2.2.1) can be found in Table 4. Overall this ice modeling approach achieves an excellent match between flight data and model output. Figure 14 and Figure 15 show the similar time histories, lift curve slope and drag polar, but in this case for the flight test with configuration SLD III.

Despite a more extensive icing condition the covered AOA range from -1 deg to 7 deg is larger so that a slight nonlinearity in the upper AOA region is visible, but was not truely identifiable with the parameters which were set free for estimation. Apart from that, a difference between the clean and icing lift characteristic is not measurable.

Parameter	SLD I	SLD III
k_{CD0}	0.980	1.182
d_{k1}	-0.048	-0.074
d_{k2}	0.661	1.474
k_{α^*}	-0.281	-0.304

Table 4: Estimated icing drag Δ-model parameters.

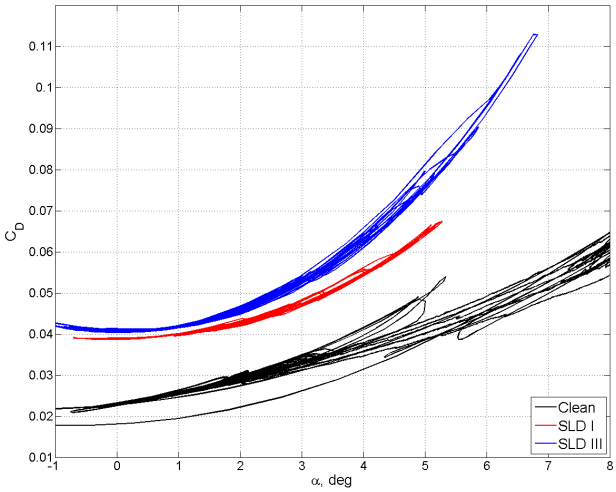

Figure 16: Drag versus AOA comparison: Clean Configu ration – SLD I – SLD III.

The increase of the drag at zero lift component is very significant: It is about 120% higher compared to the clean aircraft (see Table 4). In difference to the SLD I case the curvature of the SLD III drag polar is significantly higher compared to the clean aircraft curve. Overall the same icing model approach is appropriate for finding a good match between flight test and simulation model output. For summarizing the longitudinal motion results cases compared to the clean aircraft simulation. Figure 16 shows the simulation model drag coefficient versus AOA for both icing cases. Here again the zero drag increase and the change in the drag polar curvature for the SLD icing cases compared to the clean aircraft case are illustrated impressively.

4.2.2. Lateral Motion

For the analysis of changes in lateral motion derivatives all times slices with lateral maneuvers were used as input for the estimation process. The evaluation of the lateral motion for the flight in SLD III configuration are exemplary presented in Figure 17 by time history plots of the six most important aircraft motion and control quantities. Overall four maneuvers are shown, two with aileron and two with rudder step inputs. The control surface deflections of the left aileron and rudder are illustrated in the lower two time histories. The upper four time histories show the aircraft roll and yaw rates p and r, the bank angle θ and the angle of sideslip β. The line color code corresponds to the longitudinal motion plots presented in the previous section.
Due to the massive drag increase in the icing flight cases the yaw damping behavior has changed significantly compared to the clean aircraft, the yaw rate amplitudes are much smaller. As mentioned in section 2.2.1 for the lateral motion Sys-ID was performed with a decoupled lateral motion model. During the Sys-ID process only the derivatives which indicated a significant contribution to a good match between flight test data and model outputs (see red and blue lines in Figure 17) were newly estimated for icing. In Table 5 the final results of this estimation process for the SLD III configuration are listed. The estimated roll damping coefficient C_{lp} shows almost no deviation from the clean aircraft parameter value. The weathercock sta-

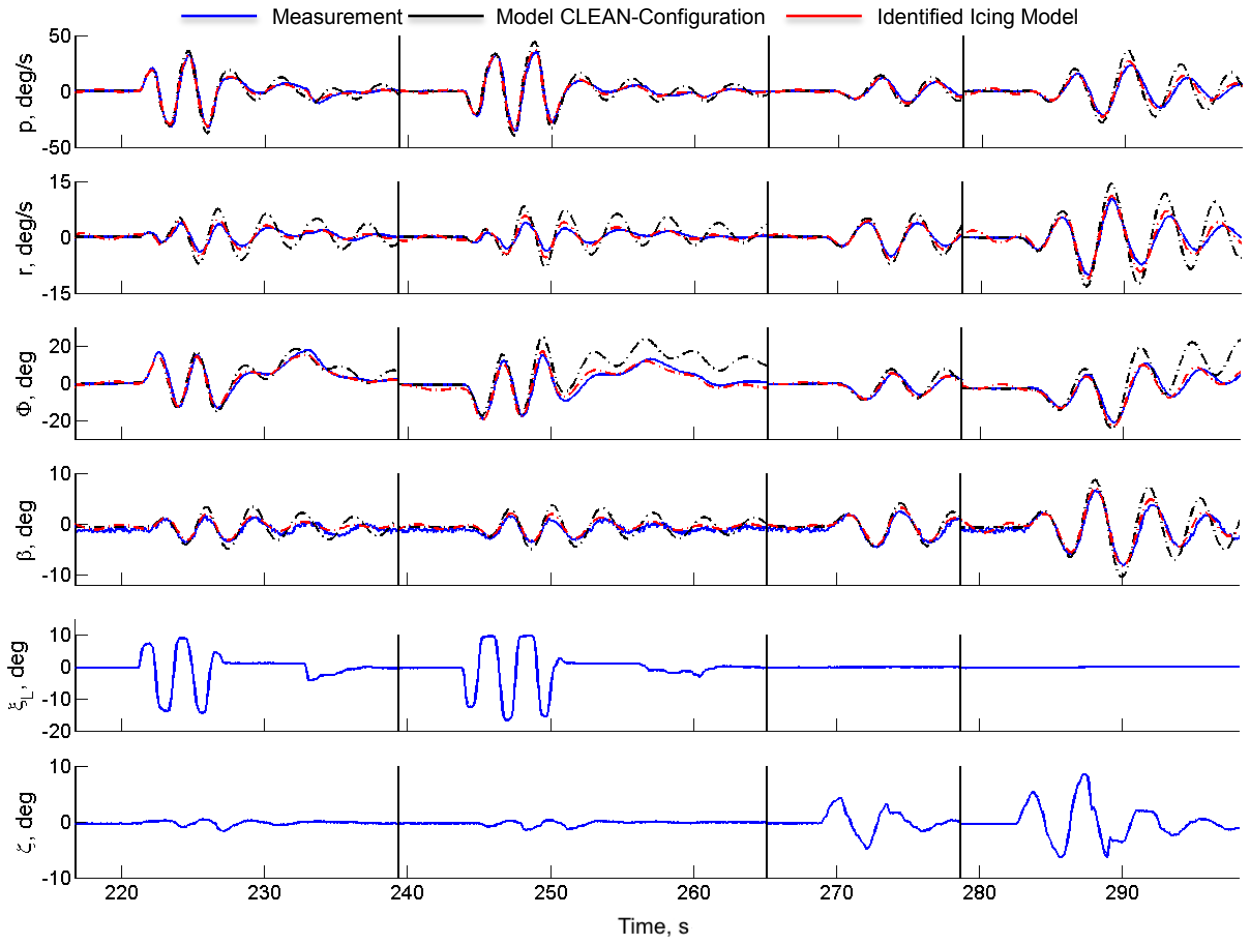

Figure 17: Lateral maneuver time histories / aileron and rudder step inputs.

bility $C_{n\beta}$ increased by nearly 3 %, presumably because of the increasing wing drag, whereas the aileron control effectiveness derivative $C_{l\xi}$ decreased by nearly 6 %.

Derivative	SLD III - Clean	Δ Clean, %	Rel. Error, %	Std. Dev.
C_{lp}	0.0068	-0.7	0.2	0.0021
C_{lr}	-0.1678	-333.8	4.5	0.0053
$C_{l\xi}$	0.0079	-5.8	0.3	0.0004
$C_{n\beta}$	0.0053	2.8	0.1	0.0001
C_{np}	0.0456	-108.8	12.5	0.0005
C_{nr}	-0.1259	36.9	0.4	0.0016

Table 5: Lateral model parameter change due to SLD III icing.

More pronounced is the change in the yaw damping coefficient C_{nr} which increases by almost 40 % due to the increased wing drag with ice shaped attached.
The most significant deviations from the clean aircraft state can be seen in the results for the yaw-roll coupling derivatives C_{lr} and C_{np} showing a reduction of more than 100 %. However the relative error for these estimates is quite high when compared to the other derivatives. Moreover, the corresponding derivative values for the clean model are quite small, and were difficult to obtain during the clean aircraft Sys-ID. For this reason the effects of the icing shapes yaw-roll coupling cannot be determined exactly and must be analyzed further. Despite these high standard deviations a very good match between the aerodynamic model and the flight data was achieved as can be seen in the plots of Figure 17.

5. Summary and Conclusion

New certification rules and the intention to understand the phenomena of SLD icing lead to research cooperation between the German Aerospace Center (DLR) and EMBRAER. Flight tests with a Phenom 300 aircraft in clean configuration and in a configuration equipped with artificial ice shapes were performed in order to identify an aerodynamic model which could be used in a high-fidelity flight simulation. The flight tests were supported by online parameter estimation tools which allowed detecting changes in the aircraft aerodynamic within seconds during the flight and leading to a faster verification of results from wind tunnel experiments and CFD calculations conducted before the flight with ice shapes. The SLD ice shapes increased the aircraft drag by more than 70 % when compared to the clean aircraft under the same flight condition. Almost no effects could be detected on the lift characteristics; however this has to be investigated with additional flight maneuvers at higher angles of attack. The online tool RAPIT was able to detect the changes in the aircraft performance within seconds during the flight. Results were confirmed by FITLAB-Online which estimated an aerodynamic Δ-model using all maneuvers. A direct comparison of the outputs of an aerodynamic model identified from the clean aircraft data and the newly identified icing model already at the debriefing gave insights on the aerodynamic changes of the aircraft and supported further decision making. Both tools detected a reduction in aileron effectiveness around 6 to 7 % which is in good accordance with the results from wind tunnel results. The growth in drag on the aircraft wings led to significant changes in the yaw dynamics. A massive increase in yaw damping was detected with both online parameter estimation tools, whereas no major changes in the weathercock stability were determined. The yaw-roll coupling dynamics will be scope of further investigations using more detailed offline parameter estimation algorithms.
Experiences gained with the online parameter estimation tools during the flight test campaign confirmed their usefulness for the support of the flight test crew. Flight safety was increased because pre-flight information about the aerodynamic characteristics could be confirmed during the first maneuvers and critical performance parameters could be monitored directly. Decisions on how to proceed could be taken much faster because information about the level of aerodynamic alteration was already available at the debriefing of the flight. Online processing of flight data in order to make the flight test more safe and efficient will be the scope of ongoing research at DLR Institute of Flight System.

ACKNOWLEDGEMENT

The authors would like to thank the Flight Test Division at EMBRAER for giving the opportunity of being part in the SLD flight test program and the Flight Data Processing Group for helping with the data interface and installations.

REFERENCES

[1] Bernstein, B. C., Campo W., Algodoal, A., Bottino, F., Lilie, L., and Agostinho, H., “The EMBRAER-170 and -190 Natural Icing Flight Campaigns: Keys to Success,” *44th AIAA Aerospace Science Meeting and Exhibit*, 9 – 12 January 2006, Reno, Nevada, Paper No. AIAA 2006-264, American Institute of Aeronautics and Astronautics, 2006.

[2] Bragg, M. B., Hutchison, T., Merret, J., Oltman, R., and Pokhariyal, D., “Effect of Ice Accretion on Aircraft Flight Dynamics,” *38th AIAA Aerospace Science Meeting and Exhibit*, Reno, Nevada, USA, January 10th 13th, 2000. American Institute of Aeronautics and Astronautics, Inc. (AIAA), Paper No. AIAA 20000360.

[3] Brandon, J. M. and Morelli, E. A., “Real-Time Onboard Global Nonlinear Aerodynamic Modeling from Flight Data,” *AIAA Atmospheric Flight Mechanics Conference*, 16 – 18 August 2014, Atlanta, GA, Paper No. AIAA 2014-2554, American Institute of Aeronautics and Astronautics, Inc. (AIAA), 2016

[4] Deiler C., „An Online Parameter Estimation Tool. No. 1206,“ *Deutscher Luft- und Raumfahrtkongress, Deutsche Gesellschaft für Luft- und Raumfahrt*, Berlin, Germany, September 10th - 12th 2012.

[5] Deiler, C., “Aerodynamic Modeling, System Identification and Analysis of Iced Aircraft Configurations”, *AIAA Atmospheric Flight Mechanics Conference Washington D. C.*, AIAA Aviation, Paper No. AIAA 2016-3852, American Institute of Aeronautics and Astronautics, Inc. (AIAA), 2016.

[6] Deiler, C., “Data parser approaches for (online) parameter estimation,” *CEAS Aeronautical Journal*, Vol. 5, No. 3, pp. 345-357, September 2014, Council of European Aerospace Societies, Springer Vienna.

[7] Deiler, C., “Time Domain Output Error System Identification Of Iced Aircraft Aerodynamics,” *Deutscher Luft- und Raumfahrtkongress, Deutsche Gesellschaft für Luft- und Raumfahrt*, Rostock, Germany, September 22th - 24th 2015.

[8] Deters, W. D; Glen, A. D. and Selig, M. S., ”Icing Encounter Flight Simulator,” *AIAA, Journal of Aircraft*, Vol. 43, No. 5, September – October 2006, American Institute of Aeronautics and Astronautics, Reston, VA.

[9] Etkin, B. and Reid, L. D., *Dynamics of Flight – Stability and Control*, 3rd edition, John Wiley & Sons, Inc., New York, 1996.

[10] Green, S. D., “A Study of U. S. Inflight Icing Accidents and Incidents, 1978 to 2002,” *44th AIAA Aerospace Sciences Meeting and Exhibit 9 -12 January 2006*, Reno, Nevada, Paper No. AIAA 2006-82, American Institute of Aeronautics and Astronautics, Inc. (AIAA), 2006.

[11] Jategaonkar, R. V., *Flight Vehicle System Identification: A Time Domain Methodology*, American Institute of Aeronautics and Astronautics, Reston, VA, 2006.

[12] Klein, V. and Morelli, E., *Aircraft System Identification: Theory and Practice*, American Institute of Aeronautics and Astronautics, Reston , VA, 2006.

[13] Laban, M., *On-line aircraft aerodynamic model identification*, Dissertation, Technical University Delft, Delft, The Netherlands, 1994.

[14] Martin, J. C. T., “The Adverse Aerodynamic Effects of Inflight Icing on Airplane Operation,” *Aviation Safety Newsletter*, Issue 1/2007, TP185E, Transport Canada, Civil Aviation, Ottawa, 2007.

[15] Morelli, E. A., “Flight Test Maneuvers for Efficient Aerodynamic Modelling,” Paper No. 2011-6672*, AIAA Atmospheric Flight Mechanics Conference*, Portland, Oregon, 2011.

[16] Morelli, E. A., “Real-Time Aerodynamic Parameter Estimation in the Frequency Domain,” *AIAA Journal of Guidance, Control and Dynamics*, Vol. 23, No. 5, American Institute of Aeronautics and Astronautics, Reston, VA, 2000

[17] N. N., Advisory Circular 25-28, *Compliance of Transport Category Airplanes with Certification Requirements for Flight Icing Conditions*, U. S. Department of Transport, Federal Aviation Administration, AC 25-28, 27th October 2014, Washington D. C.

[18] N. N., *Part 25—Airworthiness Standards Transport Category Airplanes*, U. S. Department of Transport, Federal Aviation Administration, 6th July 2016, Washington D. C.

[19] N. N., *Wind-Tunnel Measured Aerodynamic Effects on the Phenom 300 due to SLD Ice Accretion*, Technical Report, DT1OTY006, EMBRAER, São José dos Campos, 2015

[20] National Aeronautics and Space Administration, ”Parameter Estimation Techniques and Applications in Aircraft Flight Testing – A Symposium at the NASA Flight Research Center,” April 24-25, 1973,” NASA, Technical Note, TN D-7647, Washington, D. C., 1974

[21] Raab C., “RAPIT - Rapid Aerodynamic Parameter Identification Tool, Development and Application Examples, Version 1.0,” Technical Report, IB 111-2012/80, DLR, Institut für Flugsystemtechnik, Braunschweig, 2012.

[22] Raab, C., “Rapid Aerodynamic Parameter Identification on a Large Transport Aircraft,” *AIAA SCITECH 2014, Atmospheric Flight Mechanics Conference*, 13.-17. Jan. 2014, National Harbor, Maryland, USA, ISSN 0021-8669, American Institute of Aeronautics and Astronautics, Inc. (AIAA), 2014.

[23] Ratvasky, T. P. and Ranuado, Richard J., “Icing Effects on Aircraft Stability and Control Determined from Flight Data. Preliminary Results,” *31st AIAA Aerospace Science Meeting and Exhibit*, Reno, Nevada, USA, January 11th 14th, 1993. American Institute of Aeronautics and Astronautics, Inc. (AIAA), Paper No. AIAA 930398.

[24] Ratvasky, T. P.; Barnhart, B. P. and Lee, S, “Current Methods Modeling and Simulating Icing Effects on Aircraft Performance, Stability and Control,” *AIAA, Journal of Aircraft*, Vol. 47, No. 1, January – February 2010, American Institute of Aeronautics and Astronautics, Reston, VA.

[25] Ratvasky, T. P.; Barnhart, Billy P.; Lee, Sam and Cooper, Jon, “Flight Testing an Iced Business Jet for Flight Simulation Model Validation,” *45st AIAA Aerospace Science Meeting and Exhibit, Reno, Nevada*, USA, January 8th 11th, 2007. American Institute of Aeronautics and Astronautics, Inc. (AIAA), Paper No. AIAA20070089.

[26] Seher-Weiss, S., “FITLABGUI – A Versatile Tool For Data Analysis, System Identfication and Helicopter Handling Qualities Analysis,” *42nd European Rotorcraft Forum*, September 5 – 8, 2016, Lille, France.

[27] Spaulding, T., Naddy, C., Knowlan, G., Hines, J., Schaffer, Z., Riley, D., and Jorris, T., “Near Real-time Parameter Estimation in the C-12C,” AIAA 2011-6275, *AIAA Atmospheric Flight Mechanics Conference*, American Institute of Aeronautics and Astronautics, Portland, Oregon, 2011.